# Prediction of Neutron Emission Anisotropy for Validation of an Analysis Model for Neutron Spectra in Beam-Injected LHD Deuterium Plasmas[*]

Shota SUGIYAMA, Hideaki MATSUURA, Takuya GOTO[1,2], Takeo NISHITANI[1], Mitsutaka ISOBE[1,2] and Kunihiro OGAWA[1,2]

*Applied Quantum Physics and Nuclear Engineering, Kyushu University, 744 Motooka, Fukuoka 819-0395, Japan*
[1]*National Institute for Fusion Science, National Institutes of Natural Sciences, 322-6 Oroshi-cho, Toki 509-5292, Japan*
[2]*SOKENDAI (The Graduate University for Advanced Studies), 322-6 Oroshi-cho, Toki 509-5292, Japan*

We developed an analysis model to predict and describe neutron emission anisotropy caused by anisotropy of energetic deuterons in the large helical device (LHD), by considering energetic-ion distribution functions, the differential cross-section of fusion reactions, and the exact shape of the vacuum vessel of the LHD. Neutron emission anisotropy that can be observed by the neutron activation system is evaluated numerically assuming deuterium-beam-injected deuterium plasmas confined by the LHD using the model. We demonstrate the dependence of neutron emission anisotropy on the beam-injection direction and the electron temperature. Based on this estimation, we propose an experimental scenario to validate the analysis model and easily understand energetic-ion anisotropy caused by the neutral beam injection.

## 1. Introduction

Energetic ions generated by external heating and fusion reactions form non-Maxwellian tails in ion distribution functions in burning plasmas [1–3]. Electromagnetic field perturbations associated with Alfvén eigenmodes can also create non-Maxwellian tails by distorting bulk-ion distribution functions [4]. These tails can affect the ignition condition [5]. The growth rate of instabilities driven by energetic particles depends on their radial profile and energy distribution. It is therefore important to understand the nature of non-Maxwellian tails created by various phenomena both theoretically and experimentally.

As neutrons are emitted mainly from the reaction of energetic ions in neutral beam (NB)-injected deuterium plasmas confined by current experimental devices, we can obtain information on confined energetic ions by neutron measurements. The large helical device (LHD) has several neutron measurement systems, including the neutron flux monitor (NFM) [6] and the neutron activation system (NAS) [7]. The NFM measures the time-dependent total neutron emission rate using a $^{235}U$ fission chamber, $^{10}B$, and two $^{3}He$ counters, whereas the NAS counts the number of neutrons during a shot using the activation foils. Energetic-particle physics studies on the basis of neutron measurements have been performed, such as the so-called triton burnup and NB-blip experiments in the LHD deuterium plasma experiment [8, 9]. In deuterium-beam-injected deuterium plasmas, as the NB is injected in a particular direction, the deuteron velocity distribution function has an anisotropic non-Maxwellian tail. As a consequence of the formation of the anisotropic tails, the emission spectra of fusion-produced neutrons are modified from the Gaussian distribution, having anisotropic non-Gaussian components [10, 11]. Neutron emission anisotropy has been experimentally confirmed by both the NFM and the NAS in the LHD [12].

We have developed an analysis model that is capable of evaluating the neutron flux, incident energy, and angle distributions at arbitrary positions along the vacuum vessel [11, 13]. This model considers fuel-ion distribution functions, the differential fusion cross-section, and the exact shape of the vacuum vessel of the LHD. Employing this model, neutron emission anisotropy observed in the LHD can be described systematically, and we can further understand the energetic-ion physics related to the shape of the deuteron distribution function in stellarator devices. Understanding of neutron emission anisotropy might provide useful information for the neutronic design of the LHD-type DEMO reactor [14]. To discuss various phenomena that cause neutron emission anisotropy, our model has to be validated with experimental results.

The purposes of this paper are to establish an analysis model that predicts and explains neutron emission anisotropy, and to propose possible experiments to validate the model based on a qualitative prediction of the plasma temperature and density dependences of neutron anisotropy, assuming NB-injected LHD deuterium plasmas. The neutron rate that directly enters activation foils employed for the NAS from a beam-injected LHD deuterium plasma, is evaluated under several plasma conditions. We predict the dependence of the ratio of the neutron rate measured by the activation foil installed at an outside port (8-O port) to that installed at a lower vertical port (2.5-L port) on the NB-injection direction and the electron temperature. Based on this prediction, we propose possible experiments to validate our analysis model and to understand the dependence of neutron emission anisotropy.

## 2. Analysis Model

The distribution function of energetic deuterons generated by an NB injection is evaluated following guiding-center orbits of test particles using the DELTA5D code [15] as follows [11]:

$$
f\left(\mathbf{v}, \frac{r}{a}\right) d\mathbf{v} dV = \sum_{i=1}^{N_p} \sum_{j=1}^{N_t} \frac{S_{\text{NBI}} \Delta t}{N_p} \\
\times \delta'\left(\mathbf{v} - \mathbf{v}_{i,j}\right) \delta'\left[\frac{r}{a} - \left(\frac{r}{a}\right)_{i,j}\right],
\tag{1}
$$

where $f$ is the distribution function, $\mathbf{v}$ is the velocity of a test particle, $r/a$ is the normalized minor radius, $V$ is the plasma volume, $N_p$ is the number of test particles, $N_t$ is the number of time steps of the particle orbit calculation, $S_{\text{NBI}} = P_{\text{NBI}}/E_{\text{NBI}}$, $P_{\text{NBI}}$ is the NB-injection power, $E_{\text{NBI}}$ is the NB-injection energy, $\Delta t$ is the time step interval of the particle orbit calculation, and $\delta'$ is a dimensionless function similar to the delta function, where $\delta'(0) = 1$. The subscripts $i$ and $j$ represent the $i$-th test particle and the $j$-th time step, respectively. The equilibrium magnetic field is calculated using the VMEC [16], and the initial distribution of NB-generated deuterons is calculated by the FIT3D code [17]. The orbit of each test particle is followed until the particle either reaches the last flux surface or slows down to 1.5 times the ion temperature.

The neutron emission spectrum is defined as follows [10]:

$$
\frac{d^2 N(E_n, \chi, r/a)}{dE d\Omega_\chi} = \iiint d\mathbf{v}_d d\mathbf{v}'_d d\Omega_\zeta \frac{d\sigma}{d\Omega_\zeta} v_r \\
\times f_d\left(\mathbf{v}_d, \frac{r}{a}\right) f'_d\left(\mathbf{v}'_d, \frac{r}{a}\right) \delta(E - E_n) \delta(\Omega_\chi - \Omega_{\chi,n}),
\tag{2}
$$

where $N$ is the neutron emission rate per unit time per unit volume at a flux surface of $r/a$, $\chi$ is the neutron emission angle relative to the toroidal axis, $\zeta$ is the neutron emission angle in the center-of-mass system, $\Omega$ is the

solid angle, $d\sigma/d\Omega_\zeta$ is the differential cross-section of the D(d, n)$^3$He reaction, $v_r$ is the relative velocity of two reacting deuterons, and $\delta$ is the delta function. $E_n$ is the neutron emission energy calculated by the following formula [18]:

$$
E_n = \frac{1}{2} m_n v_c^2 + \frac{m_{^3\text{He}}}{m_n + m_{^3\text{He}}} (Q + E_r) \\
+ v_c \cos\zeta \left[\frac{2 m_n m_{^3\text{He}}}{m_n + m_{^3\text{He}}} (Q + E_r)\right]^{1/2},
\tag{3}
$$

where $m_{n(^3\text{He})}$ is the neutron ($^3$He) mass, $v_c$ is the center-of-mass speed, $Q$ is the reaction $Q$-value, and $E_r$ is the relative energy of two reacting deuterons. The cross-section of the D(d, n)$^3$He reaction is taken from Drosg and Schwerer [19] and Bosch and Hale [20]. In this study, only the beam-thermal reaction is considered; the energetic-deuteron distribution function estimated by Eq. (1) and Maxwellian are used for $f_d$ and $f'_d$ in Eq. (2), respectively. We evaluate the neutron emission spectrum by calculating Eq. (2) based on the Monte Carlo method [11,13]. The positions of the neutrons incident on the vacuum vessel are obtained by the neutron emission velocity calculated in the Cartesian coordinates and the function providing the exact shape of the vacuum vessel of the LHD [13].

The NAS measures neutrons during a shot by exposing the activation foils and counting the gamma-rays emitted from the exposed foils [7]. The activation foils are sent by pneumatic control systems to two irradiation ends located at the 2.5-L and 8-O ports. The geometric relationship between the vacuum vessel and the irradiation end (a) at the 2.5-L port and (b) at the 8-O port is shown in Fig. 1. The 2.45-MeV neutrons emitted from the D(d, n)$^3$He reaction can be measured selectively using indium foil. We estimate the neutron rate entering the foils from plasma directly by excluding neutrons incident to other positions on the vacuum vessel.

We assume deuterium-beam-injected deuterium plasmas confined by the LHD. The radial profiles of the density $n(r/a)$ and the temperature $T(r/a)$ are taken as follows:

$$
n\left(\frac{r}{a}\right) = n(0) \left[1 - \left(\frac{r}{a}\right)^8\right], \\
T\left(\frac{r}{a}\right) = T(0) \left[1 - \left(\frac{r}{a}\right)^2\right],
\tag{4}
$$

where $n(0)$ and $T(0)$ represent the values at the plasma center. The central electron density $n_e(0) = 10^{19}\,\text{m}^{-3}$ and the central ion temperature $T_i(0) = 1\,\text{keV}$ are supposed. Impurity ions are not taken into account; hence, the deuteron density $n_d$ is the same as the electron density. The LHD has five NB injectors: NB#1, #2, and #3 directed tangentially to the magnetic axis, and #4 and #5 directed perpendicularly to the magnetic axis [8]. We assumed the plasmas where NB#1 or NB#5 are used, and investigate the dependence of neutron emission anisotropy on the NB-injection direction. The NB-injection energy and port-through power are assumed to be $E_{\text{NBI}} = 180\,\text{keV}$
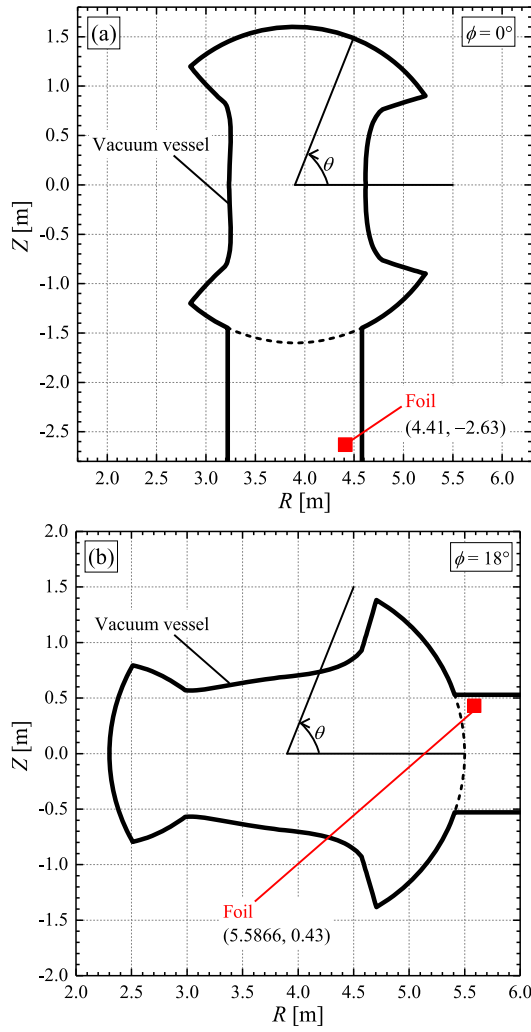
Fig. 1 Geometric relationship between the vacuum vessel and the irradiation end (a) at the 2.5-L port and (b) at the 8-O port.



Fig. 2 Volume-averaged distribution functions of energetic deuterons for NB#1 (a) with $T_e(0) = 1$ keV and (b) with $T_e(0) = 5$ keV, and for NB#5 (c) with $T_e(0) = 1$ keV and (d) with $T_e(0) = 5$ keV.

and $P_{NBI} = 5$ MW for NB#1 and $E_{NBI} = 80$ keV and $P_{NBI} = 8$ MW for NB#5, respectively.

# 3. Results and Discussion

The volume-averaged distribution functions of energetic deuterons are shown in Fig. 2 when NB#1 is injected with the central electron temperature (a) $T_e(0) = 1$ keV and (b) with $T_e(0) = 5$ keV, and when NB#5 is injected (c) with $T_e(0) = 1$ keV and (d) with $T_e(0) = 5$ keV. Here $v_{NBI}$ is the deuteron speed corresponding to the NB-injection energy, $v_\parallel$ and $v_\perp$ are the components of the deuteron velocity in directions parallel and perpendicular to the magnetic field lines, respectively. The energetic components in the deuteron distribution functions form along the direction parallel to the magnetic field for the case of the tangential NB injection (NB#1) and along the perpendicular direction for the case of the perpendicular NB injection (NB#5). Since the slowing-down time of energetic ions depends on the electron temperature, the energetic-deuteron
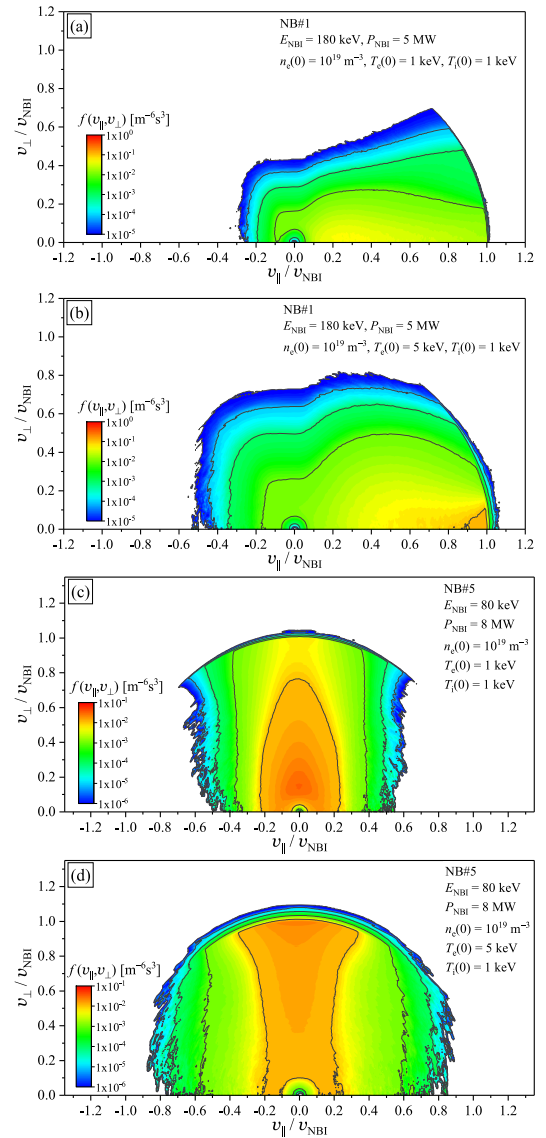
population increases as the electron temperature increases.

The volume-averaged double-differential spectra of neutrons for NB#1 (a) for all neutron emission angles $\chi$ and (c) at emission angles of $\chi = 0°$, 90°, and 180°, and for NB#5 (b) for all emission angles and (d) at emission angles of $\chi = 0°$, 45°, and 90° are shown in Fig. 3. The shape of the deuteron distribution function and the differential cross-section of the $D(d, n)^3He$ reaction cause anisotropy of the neutron emission spectrum. As shown in Eq. (3), neutrons with the maximum possible energy are emitted in the same direction as the energetic-deuteron velocity, while the minimum neutron energy is observed in the opposite direction. The injection directions of NB#1 and #5 are approximately the same as the directions $\chi = 0°$ and $\chi = 90°$, respectively. As NB#1 forms the energetic-
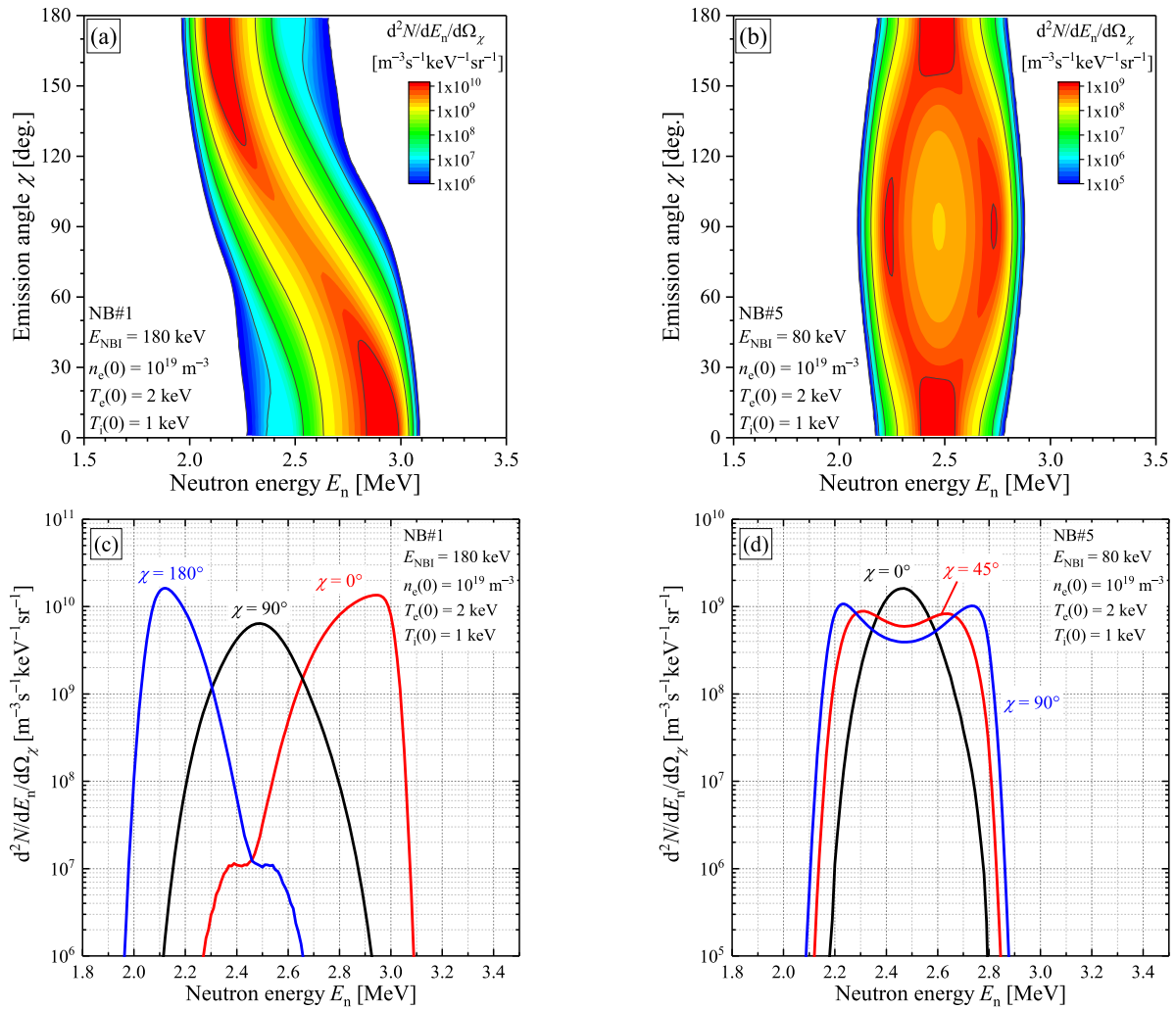
Fig. 3 Volume-averaged double-differential spectra of neutrons for NB#1 (a) for all neutron emission angles $\chi$ and (c) at emission angles of $\chi = 0°$, $90°$, and $180°$, and for NB#5 (b) for all emission angles and (d) at emission angles of $\chi = 0°$, $45°$, and $90°$.

deuteron distribution in the direction parallel to the magnetic field, the maximum neutron energy ($E_n \simeq 3.1\,\mathrm{MeV}$) is seen only in the direction $\chi = 0°$. The isotropic components of the deuteron distribution function within the velocity range $|v/v_{NBI}| \lesssim 0.4$ give rise to an energy component lower than 2.45 MeV of the spectrum at $\chi = 0°$, and a higher energy component at $\chi = 180°$. For NB#5, neutrons with the entire energy range ($2.05 \lesssim E_n \lesssim 2.9\,\mathrm{MeV}$) can be emitted in the direction $\chi = 90°$, because the gyrating energetic deuterons generated by the perpendicular NB injection produce neutrons in this direction with all the possible neutron energies. We define neutron emission anisotropy as $[2(\mathrm{d}N/\mathrm{d}\Omega_\chi)_{normalized} - 1] \times 100$ and illustrate it in Fig. 4. Here, $(\mathrm{d}N/\mathrm{d}\Omega_\chi)_{normalized}$ is the integral of the neutron emission spectra of Fig. 3 with respect to the neutron energy and normalized by the neutron emission rate. The fraction of neutrons emitted in the directions of the NB injection increases.

The neutron flux distributions normalized by the number of emitted neutrons per unit time at the positions on
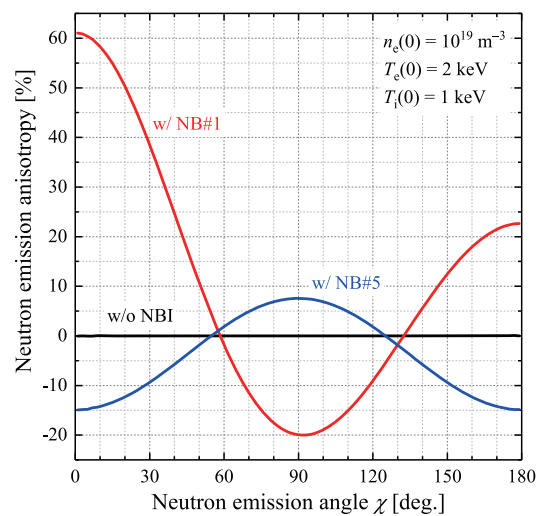


Fig. 4 Neutron emission anisotropy for NB#1, #5, and without the NB injection.

Fig. 6   Ratio $S_O/S_L$ for the cases of NB#1, #5, and without the NB injection.
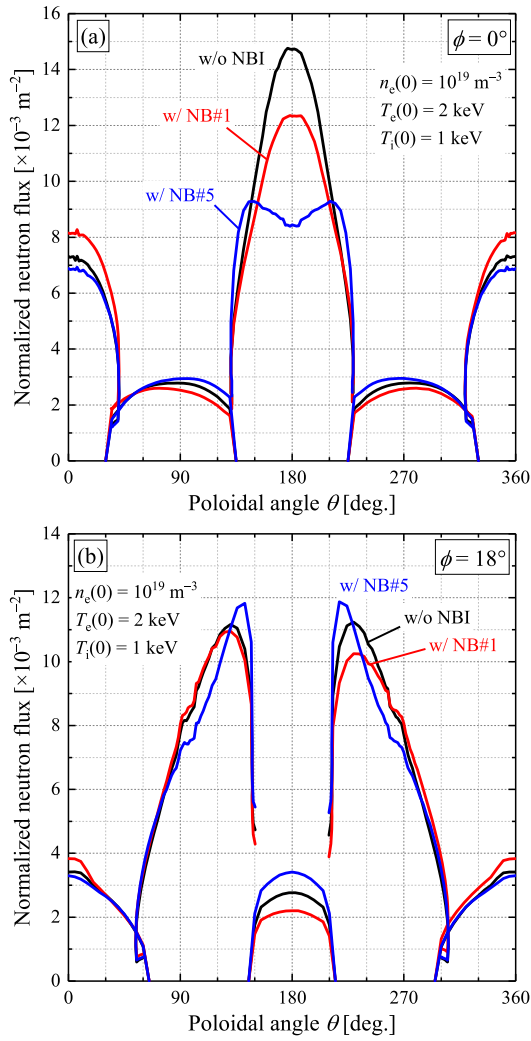
Fig. 5   Neutron flux distributions normalized by the neutron emission rate for NB#1, #5, and without the NB injection (a) at the toroidal angle $\phi = 0°$ and (b) at $\phi = 18°$.

the vacuum vessel for the cases of NB#1, #5, and without the NB injection are shown in Fig. 5 (a) at the toroidal angle $\phi = 0°$ and (b) at $\phi = 18°$. The definition of the poloidal angular wall position $\theta$ in the poloidal planes of $\phi = 0°$ and 18° is shown in Fig. 1. The flux distribution is determined by neutron emission anisotropy and the geometrical relationship between the neutron emission profile and the shape of the vacuum vessel. When no NB is injected, the geometrical relationship determines the flux distribution. In the poloidal plane of $\phi = 0°$, the flux at $\theta = 180°$ is higher than that at $\theta = 0°$, unlike in the case of tokamaks [21]. This is because the distance between the vacuum vessel and the plasma at $\theta = 180°$ is significantly shorter than that at $\theta = 0°$ owing to the complex shape of the vacuum vessel. In consideration of the neutrons emitted from the plasma center, the neutrons emitted in the directions $\chi = 0°$ and 180° can enter only the position $\theta = 0°$, while those emitted in the direction $\chi = 90°$ can geometrically enter all wall positions $\theta$. For NB#1, neutrons
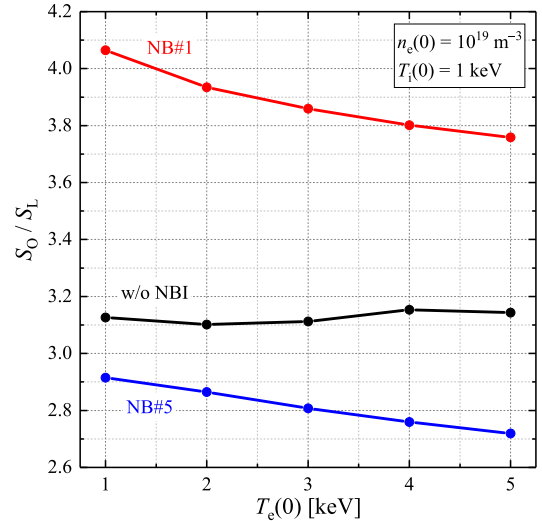
emitted in the directions $\chi = 0°$ and 180° are increased, and those emitted in the direction $\chi = 90°$ are decreased, as shown in Fig. 4. Therefore, in this case, the fraction of the neutron flux at $\theta = 0°$ increases and that at $\theta = 180°$ decreases compared to the case of isotropic emission at both poloidal planes $\phi = 0°$ and 18°. In the same manner, for NB#5, the fraction of the flux at $\theta = 0°$ decreases, whereas that at $\theta = 180°$ ought to increase compared to the isotropic case, because of neutron emission anisotropy shown in Fig. 4. However, in the plane of $\phi = 0°$, the normalized flux at $\theta = 180°$ is smaller than the case with isotropic emission. In this poloidal plane, the profile of the energetic deuteron has a peak far from the equatorial plane (the plane $Z = 0$ in Fig. 1) when the perpendicular NB is injected [22]. This energetic-deuteron profile, corresponding to the neutron emission profile, determines the fraction of the flux at $\theta = 180°$ and $\phi = 0°$ rather than neutron emission anisotropy. The locations of the irradiation ends at the 2.5-L and the 8-O ports almost correspond to the position $\theta = 281°$ and $\phi = 0°$ and the position $\theta = 14°$ and $\phi = 18°$, respectively. Hence, the ratio of neutron rates observed at the two foils provides an indication of neutron emission anisotropy.

We introduce the ratio $S_O/S_L$ as an indication of neutron emission anisotropy, where $S_{O(L)}$ is the neutron rate observed at the foil at the 8-O (or 2.5-L) port. The dependence of the ratio $S_O/S_L$ on the electron temperature for the cases of NB#1, #5, and without the NB injection is shown in Fig. 6. The neutron flux was calculated by generating 15 billion test particles for each condition, and the minimum number of particles that entered a foil was 10,423 across all conditions. Therefore, the statistical error in the Monte Carlo calculation for each point in Fig. 6 is less than 1%. The neutron rate $S_O$ increases because of neutron anisotropy when NB#1 is injected, while $S_L$ in-

creases when NB#5 is injected. Hence, the ratio $S_O/S_L$ for NB#1 is larger than the isotropic case, whereas it is smaller for NB#5. This dependence on the direction of NB injectors can be applied easily for the validation of our analysis model. The ratio $S_O/S_L$ also depends on the electron temperature for both NB#1 and #5, whereas the ratio is almost constant within the statistical error range when no NB is injected. For NB#1, the ratio approaches that of the isotropic case as the electron temperature increases, whereas the ratio for NB#5 recedes from that of the isotropic case.

Neutron emission anisotropy reflects the shape of the deuteron distribution function. Hence, the qualitative dependence of neutron emission anisotropy on the electron temperature can be roughly estimated using the slowing-down frequency $\nu_s$, the deflection frequency $\nu_d$, and the loss rate of energetic deuterons. Assuming $\nu_{i,th} \ll \nu_d \ll \nu_{e,th}$ and $n = n_e = n_d$, the temperature and density dependences of $\nu_s$ and $\nu_d$ can be written as $\nu_s \propto n/T_e^{3/2}$, $\nu_d \propto n$, where $\nu_{i(e),th}$ is the thermal speed of the background ion (electron) and $\nu_d$ is the speed of the energetic deuteron. The average energy of the confined energetic deuterons increases as $\nu_s$ decreases, because deceleration of energetic deuterons becomes slow, and the loss of deuterons that are not thermalized increases. Since anisotropy of the differential cross-section of the D(d, n)$^3$He reaction increases as the relative energy of reacting deuterons increases, neutron anisotropy is strong when $\nu_s$ is small. This effect is larger for the case of NB#5 than for the case of NB#1, because the energetic deuterons generated by NB#5 are lost easier than those generated by NB#1 due to the difference in their initial pitch angles. The anisotropy of the deuteron distribution function can be estimated by $\nu_d/\nu_s \propto T_e^{3/2}$. This ratio compares the speed of the pitch angle diffusion to the speed of thermalization of deuterons. Therefore, neutron emission anisotropy is weakened by an increase in the electron temperature for the case of NB#1, because the effect of the pitch angle diffusion is dominant. Meanwhile, anisotropy is strengthened for the case of NB#5, because the effect of the increase in average energy of the confined energetic deuterons is dominant. If this electron temperature dependence can be confirmed in experiments, our model would be validated sufficiently and can be used to interpret experimental data.

In the same manner as electron temperature dependence, we estimate the dependence of anisotropy on the ion temperature and plasma density using $\nu_s$ and $\nu_d$. The contribution of ion temperature to $\nu_s$ and $\nu_d$ is negligible. Therefore, the neutron emission anisotropy does not depend on the ion temperature. An increase in the plasma density leads to a decrease in the average energy of deuterons, while it does not affect $\nu_d/\nu_s$. Neutron emission anisotropy would weaken as the plasma density increases, regardless of the direction of the NB injection.

We focused on the neutrons that directly entered the foils after they were produced by the D(d, n)$^3$He reaction. However, the slowing down of neutrons due to scattering throughout the machine structure occurs in actual experimental plasmas. The quantitative comparison between experimental data and values shown in Fig. 6 cannot be executed in practice. The slowed-down neutrons would act as the anisotropy in the ratio $S_O/S_L$ decreases. Thus, it is necessary to investigate this effect by comparing the results obtained by our model with those obtained by the neutron transport codes such as the MCNP code [23].

## 4. Conclusion

We numerically predicted neutron emission anisotropy observable by the NAS assuming beam-injected LHD deuterium plasmas. The ratio $S_O/S_L$ of the neutron rate measured by the activation foil located at the 8-O port with respect to that at the 2.5-L port differs depending on the NB-injection direction and the electron temperature. When the NB is tangentially injected, the ratio $S_O/S_L$ is larger than the case of isotropic neutron emission and approaches the isotropic case as the electron temperature increases. For the perpendicular NB injection, the ratio is smaller than the isotropic case and leaves the isotropic case with an increase in the electron temperature. By experimentally observing these dependences of the ratio, we could validate our analysis model and discuss energetic-ion anisotropy caused by various phenomena.

## Acknowledgements

[1] J.G. Cordey and M.J. Houghton, Nucl. Fusion **13**, 215 (1973).
[2] T.H. Stix, Nucl. Fusion **15**, 737 (1975).
[3] H. Matsuura, M. Nakamura, O. Mitarai and Y. Nakao, Plasma Phys. Control. Fusion **53**, 035023 (2011).
[4] S. Sugiyama, H. Matsuura and K. Ogawa, Plasma Phys. Control. Fusion **60**, 105003 (2018).
[5] J.M. Dawson, H.P. Furth and F.H. Tenney, Phys. Rev. Lett. **26**, 1156 (1971).
[6] M. Isobe *et al.*, Rev. Sci. Instrum. **85**, 11E114 (2014).
[7] N. Pu, T. Nishitani, M. Isobe, K. Ogawa, H. Kawase, T. Tanaka, S.Y. Li, S. Yoshihashi and A. Uritani, Rev. Sci. Instrum. **88**, 113302 (2017).
[8] M. Isobe *et al.*, Nucl. Fusion **58**, 082004 (2018).
[9] T. Nishitani, K. Ogawa, N. Pu, H. Kawase, S. Murakami, M. Isobe, M. Osakabe and the LHD Experimental Group, Plasma Fusion Res. **13**, 3402024 (2018).
[10] H. Matsuura and Y. Nakao, J. Plasma Fusion Res. SERIES **9**, 48 (2010).
[11] S. Sugiyama, H. Matsuura and D. Uchiyama, Phys. Plasmas **24**, 092517 (2017).
[12] T. Nishitani, H. Matsuura, N. Pu, K. Ogawa, H. Kawase, M. Isobe and the LHD Experimental Group, IEEE Trans. Plasma Sci. **47**, 12 (2019).
[13] S. Sugiyama, H. Matsuura and T. Goto, Plasma Fusion Res. **11**, 2403049 (2016).

[14] A. Sagara *et al.*, Fusion Eng. Des. **89**, 2114 (2014).

[15] D.A. Spong, Phys. Plasmas **18**, 056109 (2011).

[16] S.P. Hirshman and J.C. Whitson, Phys. Fluids **26**, 3553 (1983).

[17] S. Murakami, N. Nakajima and M. Okamoto, Trans. Fusion Technol. **27**, 256 (1995).

[18] H. Brysk, Plasma Phys. **15**, 611 (1973).

[19] M. Drosg and O. Schwerer, Production of monoenergetic neutrons between 0.1 and 23 MeV: neutron energies and cross-sections, *Handbook of Nuclear Activation Data* (Vienna: IAEA) STI/DOC/10/273, ISBN 92-0-135087-2

(1987).

[20] H.-S. Bosch and G.M. Hale, Nucl. Fusion **32**, 611 (1992).

[21] P.P.H. Wilson, R. Feder, U. Fischer, M. Loughlin, L. Petrizzi, Y. Wu and M. Youssef, Fusion Eng. Des. **83**, 824 (2008).

[22] K. Ogawa, M. Isobe, H. Kawase, T. Nishitani, R. Seki, M. Osakabe and the LHD Experimental Group, Nucl. Fusion **58**, 044001 (2018).

[23] D. Pelowits (Ed.), MCNP6 Users Manual, LA-CP-14-00745 (Los Alamos National Laboratory, Los Alamos, 2013).